J. Fluid Mech. (1966), *vol.* 26, *part* 1, *pp.* 111–130
Printed in Great Britain

Some experiments in partially dissociated boundary layers

By P. G. SIMPKINS†
Aeronautics Department, Imperial College, London, S.W. 7

(Received 15 May 1965 and in revised form 6 December 1965)

A series of flat-plate laminar boundary layer experiments carried out in an arc-heated supersonic wind tunnel is described. Measurements of the static pressure distribution, the total pressure profiles through the boundary layer, and the heat-transfer rates to catalytic and non-catalytic surfaces at moderately high enthalpies are given and compared with various theoretical predictions. The observations indicate that the dissociation fraction affects the boundary-layer profiles through its influence on the local transport properties. It is confirmed that the atomic recombination at the surface is retarded by using a non-catalytic oxide coating, and hence the heat transfer to the wall is reduced.

1. Introduction

A considerable number of experimental investigations have been performed in high-energy laminar boundary-layer flows, primarily to study the effects of extreme temperatures on the heat-transfer rates to blunt bodies. At present, there are few data available concerning the development of a laminar boundary layer over a slender body at hypersonic velocities when the total enthalpy of the gas exceeds 1000 B.Th.U./lb. Fay & Riddell (1958) have demonstrated that, for these conditions and a wide range of altitudes, the gas-phase reactions may be neglected and thus the heterogeneous reactions play a dominant role in the mechanism of heat transfer to the surface. For chemically frozen shock layers their analysis indicates that, when the surface is a poor catalyst to the process of atomic recombination, a substantial reduction in the heat-transfer rate can be expected compared with the catalytic wall case, where the heat transfer is hardly affected by the state of the gas. The catalyticity of various materials has been examined by Goulard (1958), who has illustrated that most common metals are highly effective agents to both oxygen and nitrogen recombination, while ceramics and glasses generally have much poorer catalytic qualities.

Consider now the specific case of a flat plate situated in a partially dissociated hypersonic flow field which is chemically frozen. When atomic recombination occurs at the surface a diffusive process is maintained within the boundary layer so that the dissociation fraction at the wall c_W differs from the free-stream value c_e. Several theoretical solutions to the diffusion equation in a frozen flow field of known velocity distribution may be cited in the literature, viz. Chambré

† Present address: Aerophysics Department, Avco Research & Technology Laboratories, Wilmington, Massachusetts.

& Acrivos (1956); Chung, Liu & Mirels (1963); and Freeman & Simpkins (1965); however, a dearth of experimental data restricts any quantitative comparison. The principal difficulty of performing experiments under such conditions is that of obtaining precise measurements of local conditions in regions where both high temperatures and their gradients exist.

This paper describes such a series of experiments in a flat-plate boundary layer of a laminar non-equilibrium flow produced by an arc-heated supersonic wind tunnel. The investigations were undertaken to examine the effects of high enthalpy on the boundary-layer profiles and the rates of heat transfer to various surfaces. Initially, the experiments were performed with the model surface of a catalytic material, copper. The heat-transfer programme was subsequently repeated when the model was coated with aluminium oxide to achieve a non-catalytic surface.

2. Theoretical discussion

A body immersed in a partially dissociated flow field experiences energy transport from the boundary layer by the mechanisms of both convection and diffusion. If the free-stream composition of the gas is considered to be chemically frozen, then the total energy and momentum equations can be decoupled from the equation for the conservation of species; see Dorrance (1962). The total heat-transfer rate per unit area $\dot{q}_t$ may therefore be expressed as the sum of the convective term $\dot{q}_c$, comprised of the thermal and kinetic energies, and the diffusive term $\dot{q}_d$, representing the energy liberated by the exothermic reaction of atomic recombination. These heat-transfer rates may be independently computed when the cross-coupling between the governing equations is eliminated as in the frozen flow condition, provided a suitable assumption is made for the behaviour of the density–viscosity product.

The effects of strong viscous interaction on the rate of heat transfer to a surface have been accounted for in the work of Cheng, Hall, Golian & Hertzberg (1961). This theory may be modified for use in the weak-interaction case by introducing the first-order pressure distribution, given by $\phi = 1 + \beta\bar{\chi}$, into Cheng's result, which may be written in terms of the heat-transfer coefficient C_H as

$$C_H \left(\frac{Re_L}{C^*}\right)^{\frac{1}{2}} \simeq 0{\cdot}332\phi \left(\frac{1}{L}\int_0^x \phi\, dx\right)^{\frac{1}{2}},$$

where C^* is the constant of proportionality in the linear viscosity–temperature relationship. The resulting approximate expression for the heat-transfer rate after expanding for $2\beta\bar{\chi} \ll 1$ then becomes

$$C_H\,(Re_L/C^*)^{\frac{1}{2}} \simeq 0{\cdot}332(1-\beta^2\bar{\chi}^2).$$

Hence to first order in $\bar{\chi}$ the heat-transfer coefficient is given by the zero pressure gradient term, a result which has been noted by Hayes & Probstein (1959). The error involved in the heat-transfer rate by using a constant pressure solution when $\bar{\chi}$ is of order unity would thus be approximately 2% when $\beta \leqslant 0{\cdot}15$.

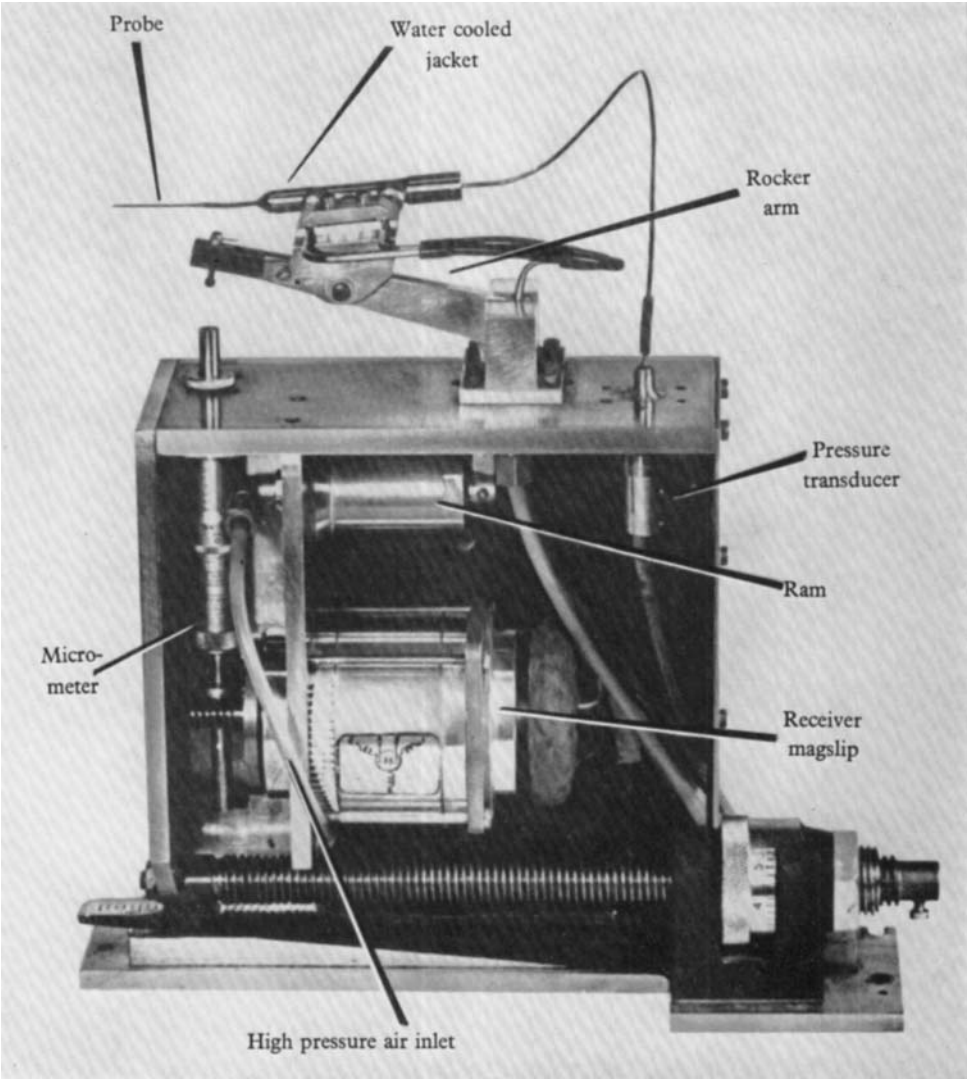

FIGURE 2. Photograph of the Pitot traverse gear.

Now, for frozen flow fields, where the chemical reactions occur only at the surface, the heat-transfer rate may be expressed as

$$-\dot{q}_t = \left[K_W \left(\frac{\partial T}{\partial y}\right)_W + \rho_W \sum_i D_i h_i \left(\frac{\partial c_i}{\partial y}\right)_W\right],$$

and by restricting ourselves to an ideal dissociating gas composed of a binary mixture of atoms and molecules—see Lighthill (1957)—the recombination term simply becomes

$$\dot{q}_d = \rho_W D_{12} h_R \left(\frac{\partial c_i}{\partial y}\right)_W.$$

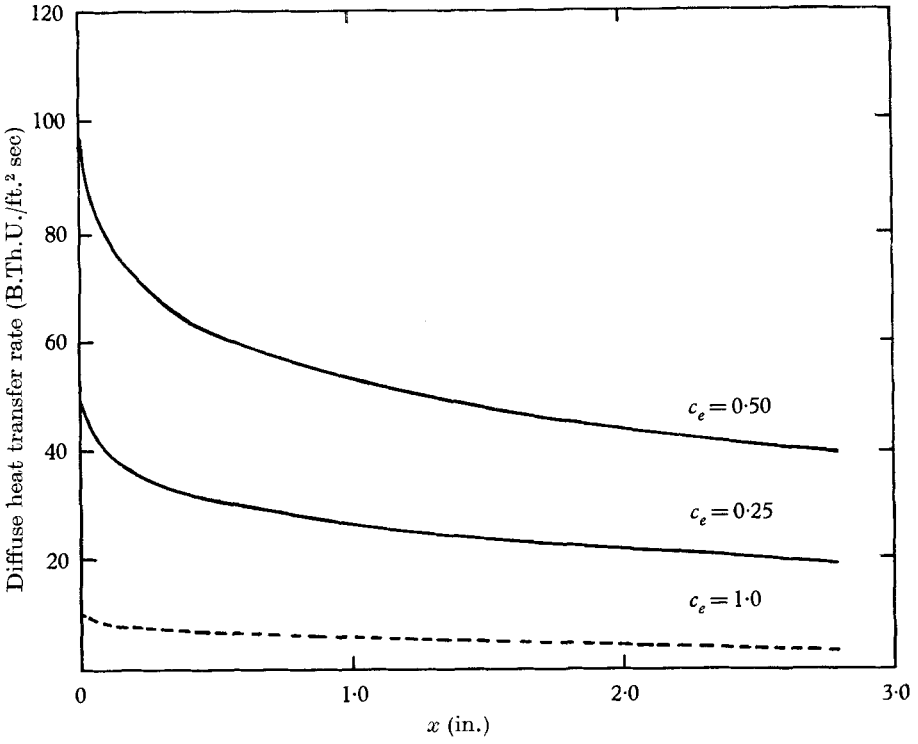

FIGURE 1. Diffusive heat-transfer rates for nitrogen. $p_\infty = 0{\cdot}01$ atm, $T_W = 500$ °K, $u_\infty = 10^4$ ft./sec, $h_R = 14{,}460$ B.Th.U./lb. ———, Copper, $K_W = 33$ ft./sec; – – –, aluminium oxide, $K_W = 1{\cdot}4$ ft./sec.

For low surface temperatures, the boundary condition follows a first-order reaction process and is given by

$$\rho_W D_{12} \left(\frac{\partial c_i}{\partial y}\right)_W = K_W \rho_W c_{iW},$$

yielding

$$\dot{q}_d = \rho_W K_W h_R c_{iW},$$

where ρ_W is the density at the surface, K_W is the wall reaction-rate coefficient and h_R the heat of recombination of the atoms. Hence the total heat-transfer rate may be finally expressed as

$$-\dot{q}_t \simeq 0{\cdot}332 \rho_\infty u_\infty (h_\infty - h_W) \left(\frac{C^*}{Re_L}\right)^{\frac{1}{2}} (1 - \beta^2 \overline{\chi}^2) + \rho_W K_W h_R c_{iW}.$$

In the cases where the effects of $\bar{\chi}$ may be neglected, the convective heat-transfer term can be calculated from any of the constant-pressure solutions. In figure 1 a series of curves for the diffusive heat-transfer rate are given, based on the data of Goulard (1958) for the various catalytic reaction-rate constants K_W, and the series solutions given by Freeman & Simpkins (1965) for the flat-plate case as

$$z = \left(\frac{c_i}{c_{i_e}}\right) = \sum_{n=0} \frac{(-1)^n}{n!} \left(\frac{\zeta}{k}\right)^n \frac{\Gamma(\frac{2}{3}(n+1))}{\Gamma(\frac{2}{3})}.$$

The notation used here is identical with that in the work cited, ζ is a transformed streamwise co-ordinate defined as

$$\zeta = \frac{K_W Sc(2\xi)^{\frac{1}{2}}}{u_e \mu_W},$$

where

$$\xi = \int_0^x \rho_e \mu_e u_e dx,$$

and k is a constant given by

$$k = \frac{2\Gamma(\frac{2}{3})(1-m)}{3\Gamma(\frac{4}{3})(1+m)} \left[\frac{Scf''(0)}{6}\right]^{\frac{1}{3}}.$$

The quantity m is the pressure-gradient parameter of the Falkner–Skan type flow, and $f''(0)$ is the shear function at the wall.

3. Experimental methods

3.1. *General description*

The experiments were performed in the arc-heated wind tunnel described by Harvey & Simpkins (1962) with argon and nitrogen gas. The principal operating characteristics of the facility are a frozen Mach number of 2·8, and total enthalpies ranging from 2000 to 8000 B.Th.U./lb. in nitrogen. The latter condition corresponds to a maximum dissociation fraction of 0·3 in the reservoir of the arc-jet.

Measurements were recorded of the static pressure distribution along the plate, the variation of Pitot pressure across the boundary layer and the heat-transfer rates to a catalytic and a non-catalytic wall. The static pressures were obtained with a silicon-oil differential multitube manometer. A pneumatic actuation, high-response Pitot probe was used to determine the boundary-layer profiles. This instrument is comprised of a ceramic tube of 0·6 mm bore and 0·2 mm wall thickness, and could be inserted and withdrawn from a known position relative to the surface in less than 0·5 sec. The pressures were determined with a strain-gauge transducer connected directly to the probe. The use of ceramic material eliminated the possibility of chemical reaction in the dissociated gas, and the thermal inertia of the probe prevented damage due to the large temperature gradients that are experienced. Accurate positioning of the probe relative to the surface entailed the use of a transmitter and receiver to achieve remote control. A photograph of the traversing mechanism is given in figure 2 (plate 1).

3.2. *Calibration procedure*

Calibration of the probe-injection gear was initially performed under normal atmospheric conditions, simply by coupling a counter to the shaft of the transmitter. The probe displacement was then recorded to within $0{\cdot}5 \times 10^{-3}$ in. for a measured angular movement of the shaft using a set of toolmaker's gauges, an electrical contact being utilized to indicate when the probe first touched a gauge of known dimensions. To verify that the probe did not distort significantly under normal operating conditions a series of photographic records of the probe displacement relative to a surface was made; it is estimated that these data incur an

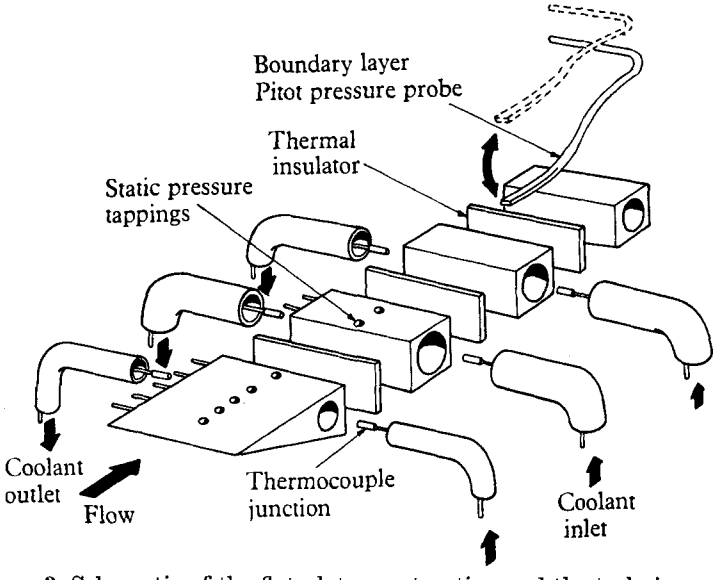

FIGURE 3. Schematic of the flat-plate construction and the techniques used in the experimental measurements.

error of $\pm 4\,\%$ when interpreted. Within this range, both sets of calibration data were in good agreement and an ultimate accuracy of $\pm 0{\cdot}0001$ in. of the probe relative to the surface is estimated under normal operating conditions.

The heat-transfer rates are determined from a steady-state process using a series of thermally insulated calorimeters—see figure 3. A pair of differential thermocouples were fitted in each calorimeter, which had a continuously calibrated supply of coolant throughout the experiments. Each pair of thermocouples were separately calibrated for a known temperature differential to within a measuring accuracy of $0{\cdot}8\,\%$. The mass-flow rates of coolant through each calorimeter were controlled by individual restrictors in each of the supply lines.

3.3. *Reduction of data*

The free-stream flow properties of the jet are based on the reservoir conditions in the arc chamber, derived from an energy-balance calculation, and the assumption of frozen isentropic nozzle flow. Spectroscopic measurements of the free-

stream temperature by Adcock & Plumtree (1964) have indicated that the nozzle flow is frozen, a conclusion which has been confirmed by Simpkins (1965) from total pressure measurements in the test section. All the theoretical calculations have used the value for the ratio of specific heats γ that is associated with the gas in its unexcited state. This represents the most realistic means of comparison with the experimental results in a régime where large temperature gradients exist. As the dissociation fraction in the nitrogen experiments was always less than 0·25, a maximum error of some 7 % could be expected in the total pressure ratios if an effective specific heat ratio defined as $\bar{\gamma} = (7 + 3c_e)/(5 + c_e)$ were used instead of the perfect-gas value; such an error is equivalent to a change in the frozen Mach number of less than 3 %. Throughout the calculations, the transport properties of Woolley (1956) and Yos (1963) have been utilized in the nitrogen analysis, in conjunction with the Mollier diagram of Humphrey, Little & Seeley (1960).

Calculations of the free-stream conditions in the argon tests are found from the known reservoir conditions by applying the Mollier diagram of Bosnjakovic, Springe, Knocke & Burgholte (1959) and the thermodynamic data computed by Arave (1963), together with the transport properties calculated by Amdur & Mason (1958).

Because of the inherent difficulty in accurately measuring the free-stream velocity the Reynolds number is calculated from an implicit value of the density–velocity product ρu obtained from the observed mass-flow rates of the gas. The Reynolds number is expressed as $Re = 21{\cdot}8(\dot{m}x/\mu)$ for the known nozzle geometry; x being a characteristic length in inches, $\dot{m}$ the gas mass-flow rate in lb./sec, and μ is the free-stream viscosity in lb./ft./sec.

The measured heat-transfer rates are mean values taken over a finite chordwise length of the plate; it is therefore necessary to define the chordwise coordinate at which to plot the experimental data. This is achieved by numerically integrating the theoretical curves of convective heat transfer to each segment of the plate, and evaluating the corresponding mean values, thus defining a unique point at which the mean heat-transfer value intersects the theoretical curve. In this way, when the diffusive effects are small the experimental results should correspond to the theoretical curve.

4. Experimental results

4.1. *The static pressure distributions*

The total pressure surveys to be discussed below revealed the existence of an axial Mach-number gradient in the free–stream, created by the model displacement effect on the jet. To minimize the effect of the pressure distribution imposed by this gradient a correction has been introduced similar to that outlined by Vas & Bogdonoff (1959) for hypersonic flows from conical nozzles. When the leading-edge shock is weak (the experiments verified the loss in total pressure to be less than 5 %) the Mach-number distribution can be found from the ratio of the total pressures (p_0'/p_0), where the subscript zero defines total conditions and the prime denotes conditions behind the probe's bow shock wave. From the above ratio

we obtain (p^*/p_0), p^* being the local static pressure of the undisturbed inviscid flow. Thus the correction factor can be expressed as the ratio of p^* at the leading edge and the local value. Symbolically, the corrected static-pressure distribution is given as

$$(p/p_\infty)_{\text{uniform}} = (p_b/p_\infty)\,(p_{x=0}/p_{x=x_1})^*,$$

where p_b is the measured static pressure at the surface, some distance x_1 from the leading edge.

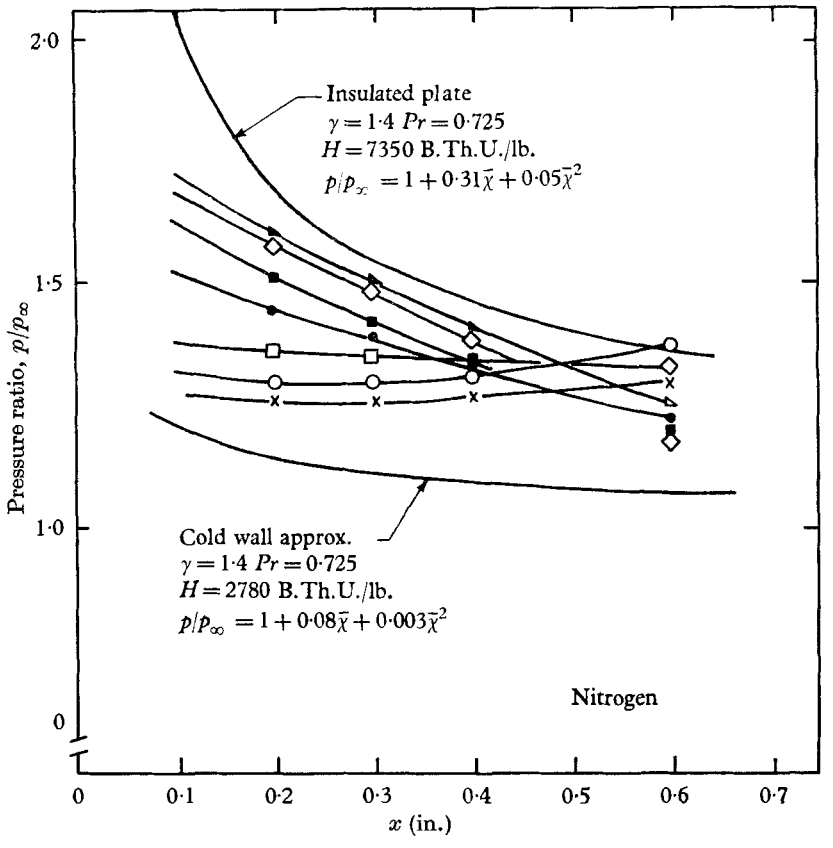

FIGURE 4. Static pressure distribution along the plate corrected for Mach-number gradient, compared with the limiting viscous interaction curves. ◣, H = 7350 B.Th.U./lb.; ◇, H = 6800 B.Th.U./lb.; ■, H = 6100 B.Th.U./lb.; ●, H = 5600 B.Th.U./lb.; □, H = 4650 B.Th.U./lb.; ○, H = 3700 B.Th.U./lb.; ×, H = 3200 B.Th.U./lb.

This correction procedure has been applied to the experimental results shown in figure 4, where a comparison is given with the weak viscous-interaction theory. The curves are similar to the cold-wall approximation at the low enthalpy levels, although it appears that the correction is somewhat excessive. As the mean total enthalpy increases, the results near the leading edge exhibit a trend towards the theoretical prediction for an insulated wall, while downstream the data are converging towards the cold-wall approximation. The comparison shows that the correction procedure results in realistic pressure distributions that are within the theoretically predicted limits. The data illustrate

that at moderate enthalpies the plate is characteristic of a cold wall, while at high enthalpies the leading edge is more like an insulated surface. This behaviour is caused by an increase in surface temperature at the leading edge due to insufficient cooling capacity at the high enthalpies. All the static pressures measured downstream of $x = 0{\cdot}7$ in. have been neglected, since at this point the results are affected by the leading-edge shock which is reflected from the edge of the jet.

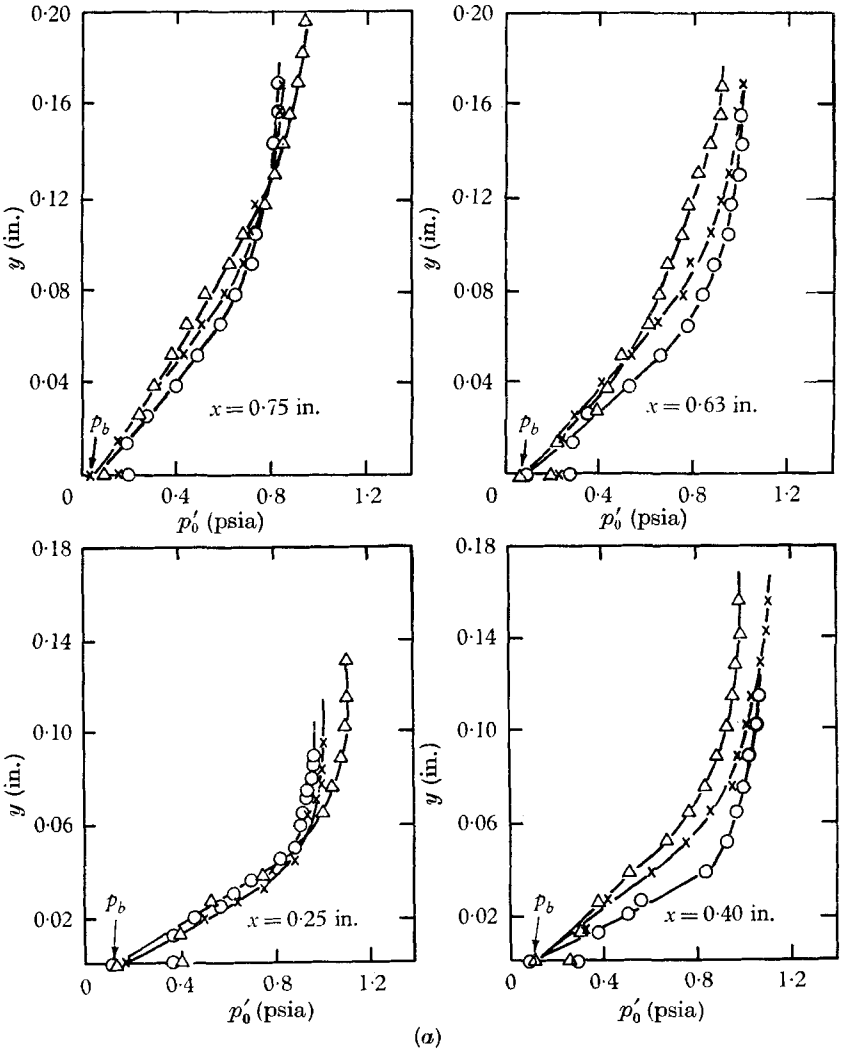

(*a*)

FIGURE 5. For legend see facing page.

Throughout these tests the plate had been set up so that it had zero incidence with respect to the nozzle geometry. A series of pressure distributions taken at angles of $\pm 1°$ and $\pm 2°$ from the zero position were recorded as a precautionary measure to indicate the existence of any incidence effects. These measurements showed that the absolute accuracy of the plate mounting was within half a degree.

4.2. *The total pressure profiles in the boundary layer*

The total pressure distributions measured throughout the nitrogen and argon boundary layers are shown in figure 5(*a*) and (*b*). As expected, the effect of increasing the mean total enthalpy of the gas is seen to result in a thickening of the

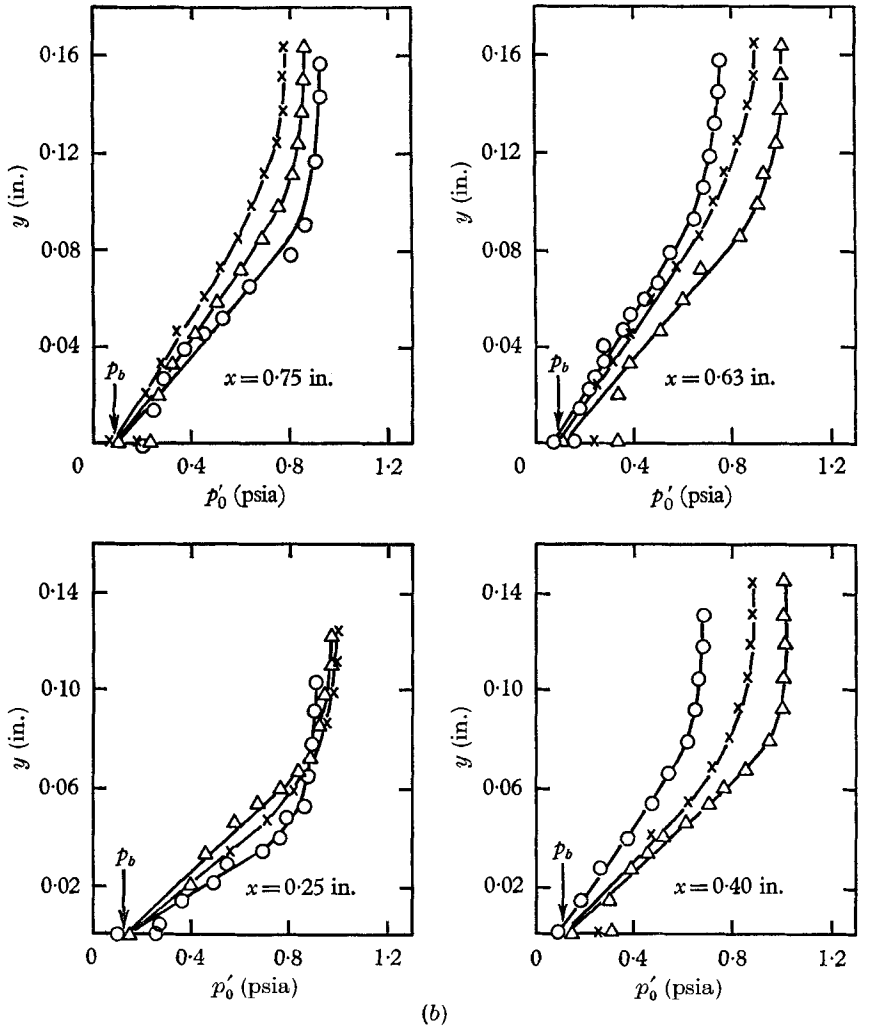

FIGURE 5. Pitot pressure distributions through (*a*) the nitrogen boundary layer: ○, H_t = 3500 B.Th.U./lb.; ×, H_t = 5880 B.Th.U./lb.; △, H_t = 6350 B.Th.U./lb.; (*b*) the argon boundary layer: ○, H_t = 870 B.Th.U./lb.; ×, H_t = 1700 B.Th.U./lb.; △, H_t = 2060 B.Th.U./lb.

boundary layer. The points p_b on the abscissa correspond to the measured static pressures on the plate during the particular tests. The distortion in profile measurements close to the wall is clearly evident; however, an extrapolation of the measured values further from the wall shows that the trend of the profiles is toward the static pressure p_b, if the distortion is ignored.

Data taken from the measured Pitot and static pressures has been used to compute the corresponding frozen Mach-number profiles in the nitrogen case, assuming the ratio of the specific heats has its perfect-gas value. Typical sets of these data taken at various chordwise positions are presented in figure 6 in their dimensionless form. The measurements have been corrected for the vorticity

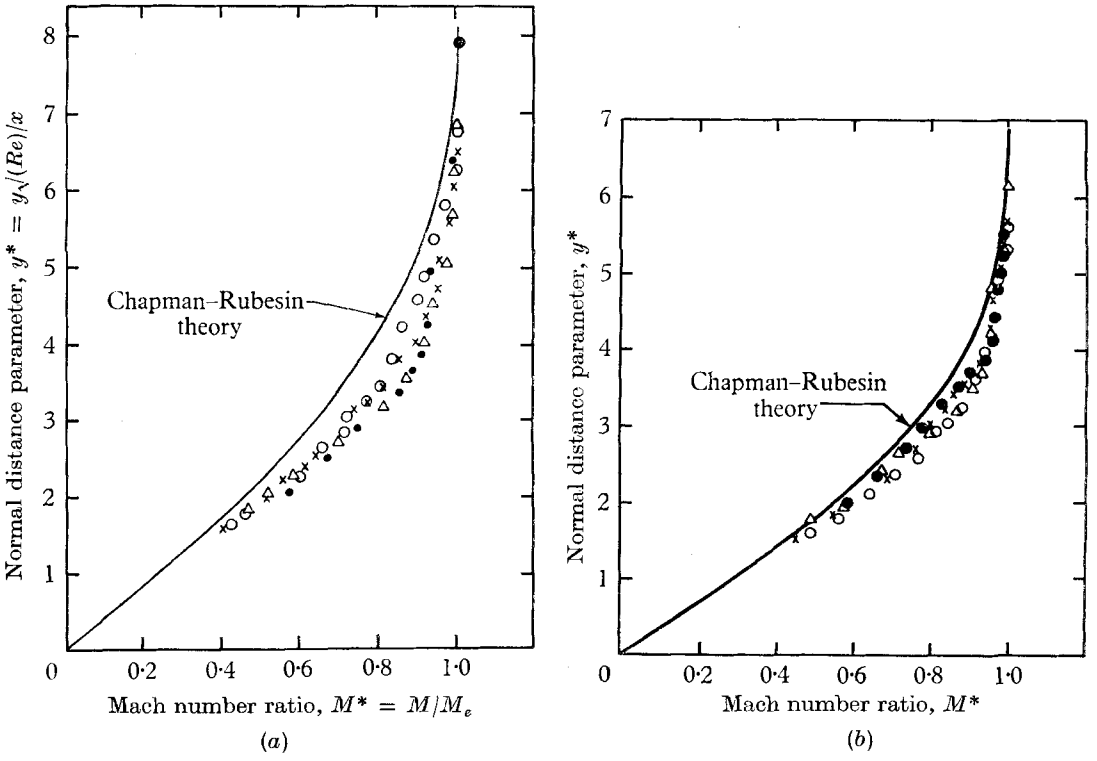

FIGURE 6. Non-dimensional profiles measured along the plate in nitrogen. ●, x = 0·25 in.; △, x = 0·40 in.; ○ = 0·63 in.; ×, x = 0·75 in. (*a*) H = 6350 B.Th.U./lb., T_e = 2700 °K, Re = 830/in. (*b*) H = 3500 B.Th.U./lb., T_e = 2350 °K, Re = 940/in.

displacement effect of the probe by transforming the normal distance parameter y^* by a linear increment Δy^* given by $k_1(dM^*/dy^*)$, the constant k_1 being evaluated at the intercept of the experimental curve with the ordinate. The profiles show a reasonable agreement in the measured Mach-number distribution, thus establishing their similarity within the limits of the experimental errors. The theoretical curves for an undissociated laminar boundary layer with zero pressure gradient due to Chapman & Rubesin (1949) at the equivalent free-stream conditions are included in figure 6 for comparison. For the high-enthalpy tests, this comparison shows a deviation of some 16 % at $y^* = 3{\cdot}5$; when the low-enthalpy results are considered, this disagreement reduces to 10 %, the free-stream dissociation fraction being reduced from 0·20 to 0·03. These comparisons will be discussed in more detail in § 5.

Estimates of the boundary-layer thicknesses based on $M_e^* = 0{\cdot}99$ are given in figures 7 and 8 for nitrogen and argon, respectively, together with the Chapman–

Rubesin predictions for a mean wall temperature of 500 °K. The agreement between the experimental curves and the theoretical predictions is reasonable, bearing in mind how strongly the correlation is affected by the chosen viscosity data. The results used here are thought to be most consistent in view of the lack of reliable information concerning viscosity at reduced pressures with significant dissociation levels. The effects of variable transport properties have recently been the subject of a paper by Janowitz & Libby (1965).

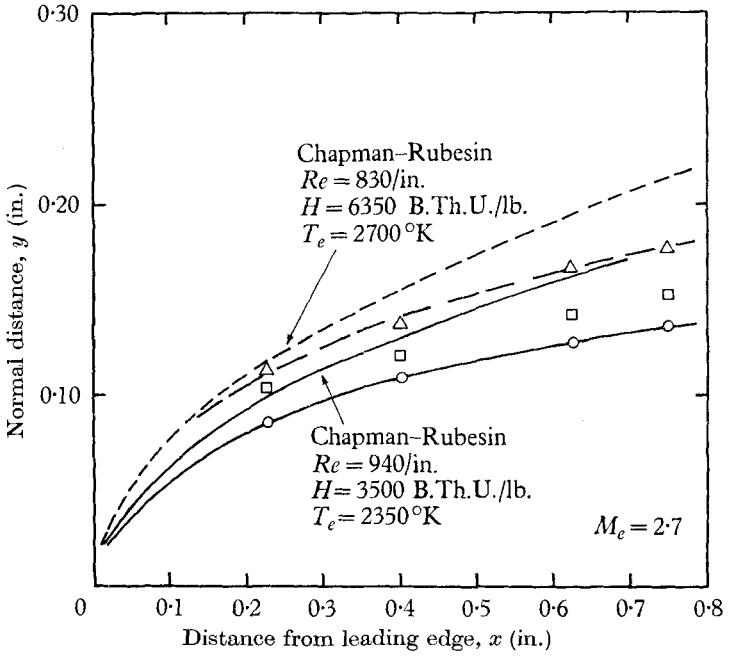

FIGURE 7. Boundary-layer growth in nitrogen.

	H (B.Th.U./lb.)	T_t °K
○	3500	5000
□	5880	5600
△	6350	5800

4.3. *Additional tests*

The displacement effect of a probe on the measured boundary-layer profile is known to be dependent on its vertical dimension—see Monaghan (1957). A number of tests were therefore carried out with a smaller probe comprised of an adjacent pair of ceramic tubes 0·7 mm in diameter, which ensured that the probe's response time was unaltered. Typical Mach-number distributions obtained with this probe are given in figure 9 and compared with the corresponding measurements taken with the larger probe. A definite profile displacement is discernible, the maximum difference being 6 % when M^* is 0·8. The effect of decreasing the vertical-probe dimension is to induce a displacement towards increasing velocity. Subsequent argon data showed similar behaviour, although one particular case gave consistent results in which the displacement was in the direction of decreasing velocity.

To establish that the flow field being examined is two-dimensional a limited number of profiles were measured for spanwise positions of 0·13 in. from the centre line. This movement is limited owing to the small scale of the test region and the knowledge that flow uniformity existed over only 0·5 in. of the jet. The results of these tests in the argon arc are shown in figure 10 and illustrate

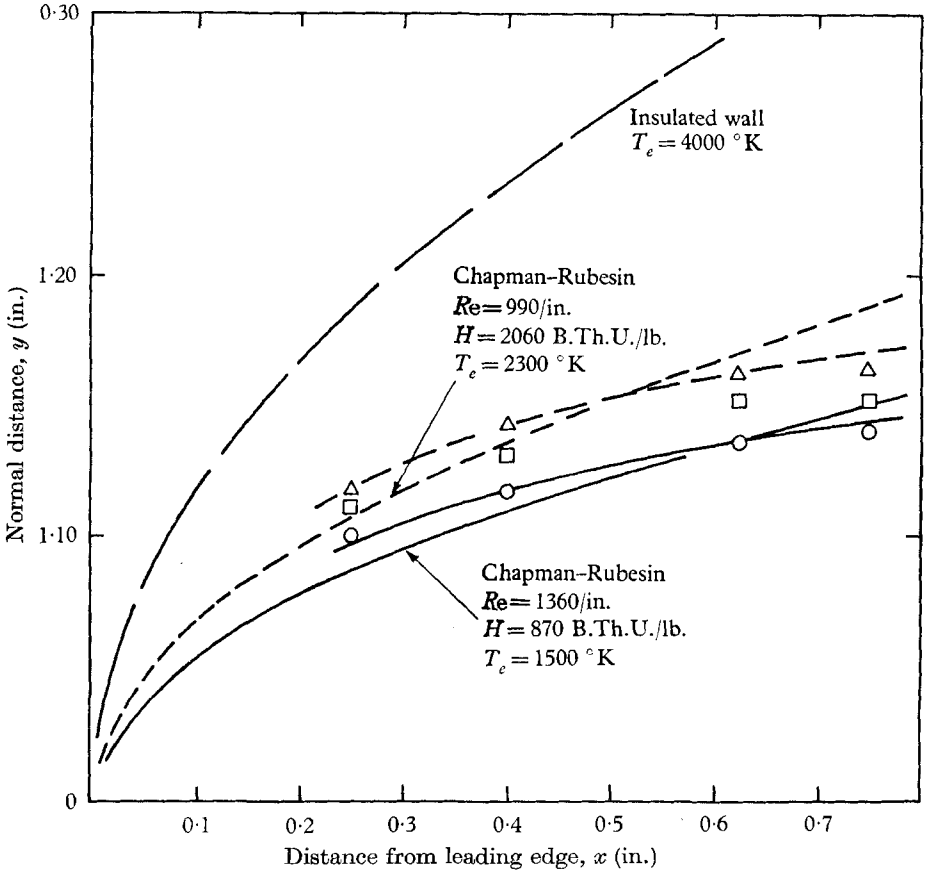

FIGURE 8. Boundary-layer growth in argon.

	H (B.Th.U./lb.)	T_t °K
○	870	4000
□	1700	7500
△	2060	8000

that the profiles are similar and in good agreement with earlier measurements, the scatter being within the predicted experimental accuracy. The values of M^* have been computed here without the vorticity correction, since we are only seeking to establish the uniformity of the flow field.

4.4. *Heat transfer results*

Quantitative measurements of the extraneous heating to the model were obtained by covering the upper surface with a water-cooled wedge to eliminate the flat-plate heat transfer. The actual heat transfer occurring to the flat plate during the

test programme was then evaluated by subtracting the extraneous heating results from the total measurement. The data shown in figure 11 illustrate the repeatibility of the leading-edge calorimeter results and also that some 50 % of the total measurement is due to under-surface heating. Similar data were obtained for the other calorimeters, although here the extraneous effects were

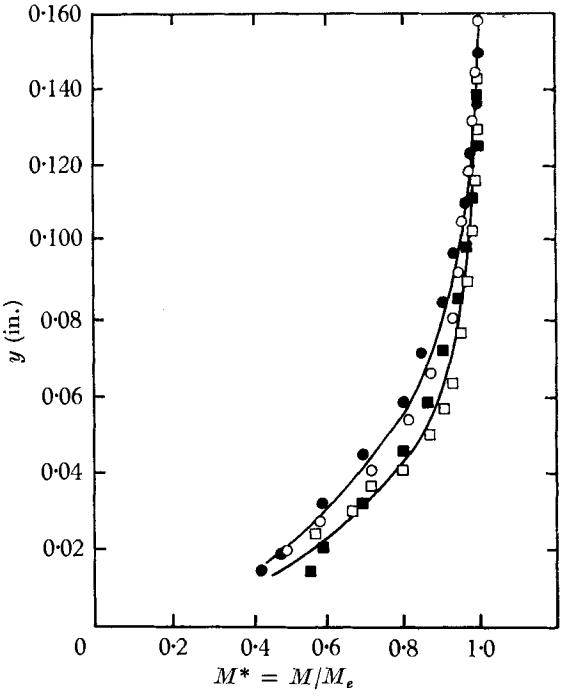

FIGURE 9. Effect of probe size on the measured nitrogen Mach-number profiles. Open symbols, d = 0·028 in.; closed symbols, d = 0·040 in. □, ■, H = 5890 B.Th.U./lb.; ○, ●, H = 7500 B.Th.U./lb.

reduced as the thermal insulation was more substantial. Note that the curves to the copper and aluminium oxide surfaces diverge as the enthalpy of the gas increases; similar measurements in argon revealed that the curves remained parallel, indicating that the oxide layer was only acting as an insulator in that case.

The results of the heat-transfer measurements on the catalytic surface in dissociated nitrogen are given in figure 12 for various enthalpy levels. In figure 13 heat-transfer results fall within the shaded area and a comparison with the solutions of Van Driest (1952) is shown for the maximum and minimum enthalpy levels. At the maximum enthalpy value of 7300 B.Th.U./lb., the theoretical curve excluding the diffusive heat transfer (viz. $c_e = 0$) is also shown. Two other curves are included which represent the series-expansion solutions for different values of K_W, the wall catalytic reaction-rate constant and a frozen dissociation fraction $c_e = 0{\cdot}25$ (this occurs at the maximum mean total enthalpy quoted above). The comparisons show that at the minimum enthalpy level there is a large difference in the theoretical and experimental data in the leading-edge

region which diminishes as x increases. When $K_W = 33$ ft./sec there is good agreement with the theoretical solution for $x > 0{\cdot}6$ in. at the maximum enthalpy level; however, approaching the leading edge the theoretical curve underestimates the experimental data. Increasing the value of K_W by a factor of five shows that better agreement is obtained in the leading-edge region, as is to be expected. It is therefore possible that the increase in wall temperature at the

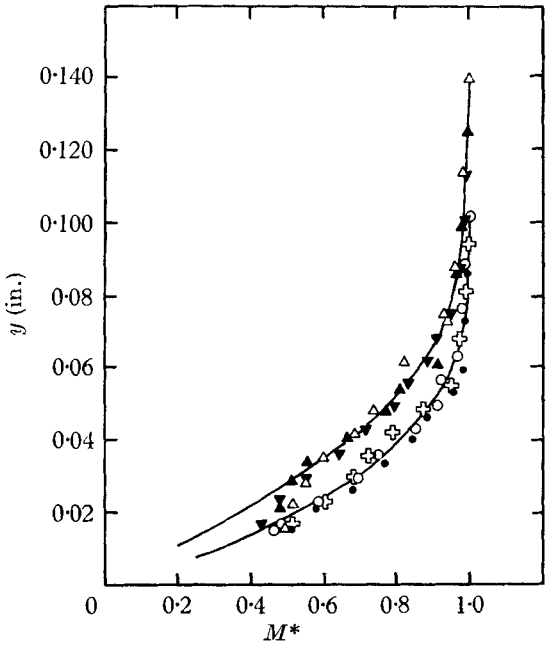

FIGURE 10. Comparison of the argon Mach-number profiles at various spanwise positions across the surface. $H = 1030$ B.Th.U./lb.

x	z	Symbol
0·25	0	○
	± 0·13	●
	− 0·13	✠
0·75	0	△
	+ 0·13	▼
	− 0·13	▲

leading edge due to inadequate cooling results in an increase in the catalytic efficiency there. Further downstream where the wall is much colder the catalyticity decreases to a value comparable to the data given by Goulard (1958). This dependence of the recombination coefficient on the surface temperature is substantiated by Prok (1963) in the case of atomic nitrogen.

The experimental results for the non-catalytic wall are given in figure 14. The diffusive heat-transfer component based on the values of K_W given by Goulard are negligible for the entire enthalpy range (i.e. less than 1 %). The upper chain-dotted curve given in the figure is derived from Van Driest's solution and a diffusive heat-transfer term based on a reaction-rate constant of 14 ft./sec. Although the agreement of both extremes of the enthalpy range is reasonable for

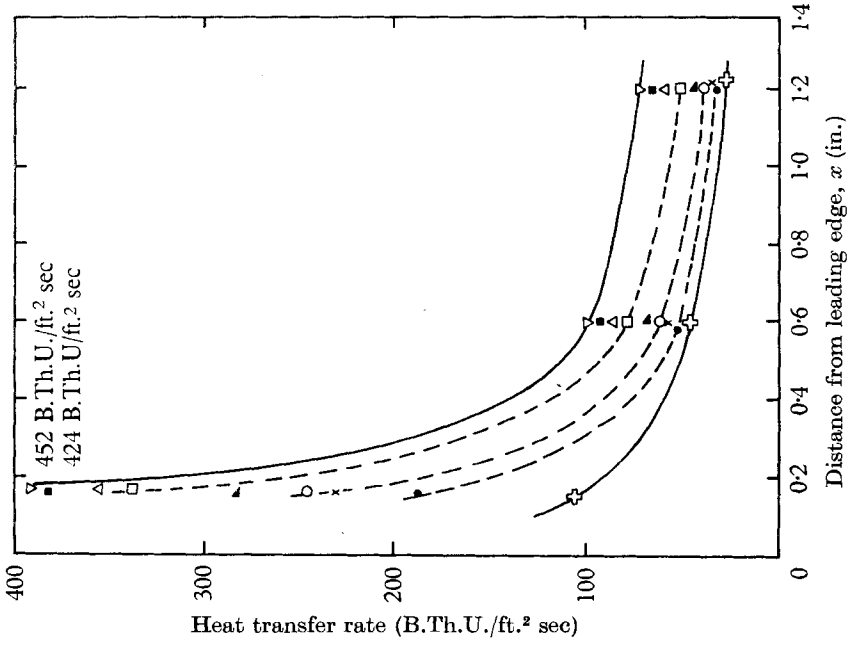

FIGURE 12. Experimental heat-transfer rates for the copper plate in nitrogen.

	H (B.Th.U./lb.)	c_e (%)		H (B.Th.U./lb.)	c_e' (%)
▽ ■	7100	25	○	4840	12
△ □	6750	23	×	4630	10
◢	6020	18	●	4140	7
	5850	16	✠	2920	2
	5260	15			

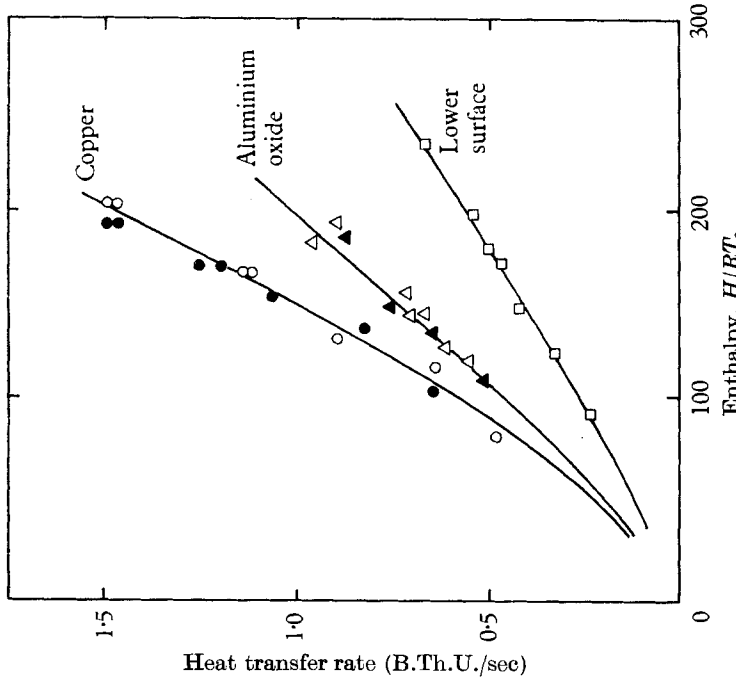

FIGURE 11. Heat-transfer rates to the leading-edge calorimeter in nitrogen.

values of x greater than 0·5 in., the leading-edge values are once more underestimated by some 25 %. The upper theoretical curve in figure 14 is truncated at $x = 0{\cdot}5$ in., since above this value the series solutions of the diffusion equation do not converge sufficiently rapidly to yield an accurate result.

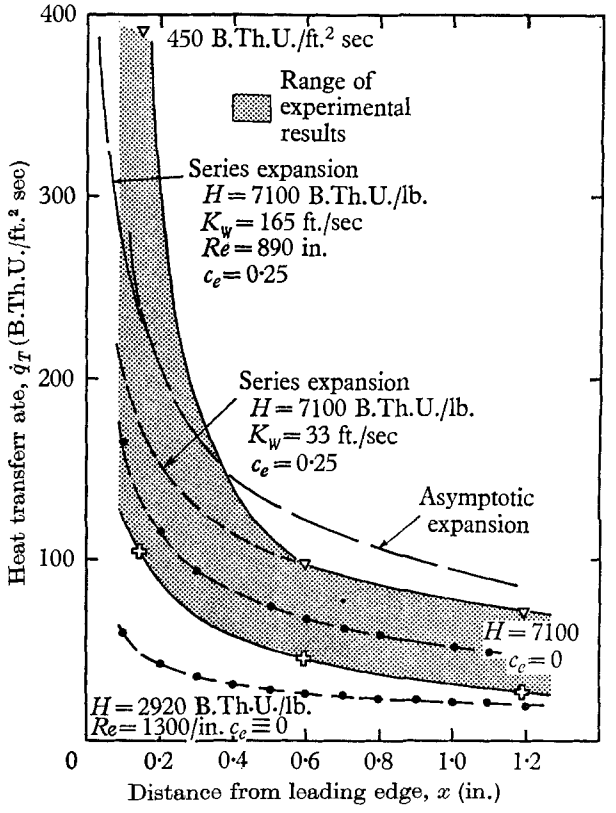

FIGURE 13. Comparison of the experimental heat-transfer results with the theoretical predictions for a catalytic surface. — —, $\dot{q}_t = \dot{q}_c + \dot{q}_d$; –●––●––●–, $\dot{q}_t = \dot{q}_c$. ▽, H = 7100 B.Th.U./lb., c_e = 25 %; ✣, H = 2920 B.Th.U./lb., c_e = 2 %.

5. Discussion

When the effects of the Mach-number gradient have been eliminated in the manner described earlier, the measurements of the static-pressure distributions compare favourably with the weak viscous-interaction theory. The effect of the free-stream enthalpy is evident from the pressure distributions shown in figure 4. Raising the enthalpy causes the distributions to depart from the cold-wall approximation and approach the insulated-surface prediction as the surface temperature increases owing to insufficient cooling. Further downstream where the surface is well cooled, the pressures approach the cold-wall approximation, upstream of the disturbance due to the reflected leading-edge shock wave, even at the high enthalpy levels.

A number of interesting points arise from the boundary-layer measurements previously described. The first of these is that substantial differences occur

between the experimental profiles and the predictions of Chapman & Rubesin, whose theory neglects dissociation effects and assumes that no pressure gradient exists. During the experiments, both of the above conditions are violated, and thus either of them, or the effect of variations in surface temperature, may be a contributing factor to the indicated discrepancies. Let us therefore consider

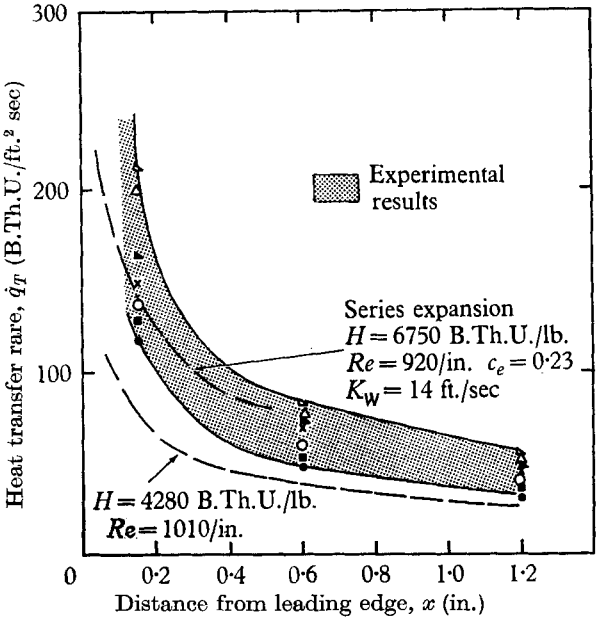

FIGURE 14. Comparison of the experimental heat-transfer results with the theoretical predictions for a non-catalytic surface.

	H (B.Th.U./lb.)	c_e (%)
◺	6750	23
△	6370	20
◣	5460	15
×	5080	14
○	4770	12
■	4520	9
●	4280	8

each of these effects separately, and examine the manner in which they affect the boundary layer. For enthalpy levels below 6500 B.Th.U./lb. the effects of the pressure gradients are negligible since the gradients themselves do not become significant until this value is approached—see figure 4. At higher enthalpy levels a comparison of the velocity profiles given by Cohen & Reshotko (1956) indicates that changes of 8–10 % in the velocity ratio from the zero-pressure-gradient condition are to be expected for the wall to free-stream enthalpy ratios under consideration. As expected, the initial slope of the velocity profile for a given wall temperature decreases as the pressure gradient becomes more favourable; i.e. the boundary layer becomes thinner. However, the differences from the zero-gradient condition are significantly larger than expected when H_t = 6500 B.Th.U./

If the low-enthalpy condition given in figure 6 is considered, a discrepancy of some 10 % in Mach-number ratio exists for a given y^*, although here the pressure gradient can be neglected.

Now consider the effects of the dissociation on the boundary-layer profiles. The profiles that have been given are all plotted against the free-stream Mach numbers, and as such include the implicit assumption that the local sound speed is frozen throughout the boundary layer. In a recent paper Janowitz & Libby (1965) have considered a boundary layer of this type, i.e. a frozen partially dissociated boundary layer with surface reaction and variable transport properties. Their results indicate that the theoretical profiles will be significantly different from the approximate solutions discussed earlier when accurate transport properties are used. The profiles themselves, for similar flow conditions to the experiments, are compressed towards the surface when the accurate transport properties are used, a behaviour which is consistent with the experimental observations outlined above.

For a given external pressure gradient, the effect of raising the surface temperature is to increase the thickness of the boundary layer. Cohen & Reshotko have observed that this effect is in the opposite sense when the transformed boundary-layer co-ordinate system is considered owing to the transformation procedure. The above behaviour may be seen in figure 7, where the percentage differences between the theoretical and experimental curves is smallest near the leading edge of the plate. Here, the assumed mean wall temperature of 500 °K is more realistic than further downstream where a highly cooled surface causes a reduction in the local boundary-layer thickness and hence a larger discrepancy from the theoretical estimates. The results from the heat-transfer investigations exhibit large differences from the theoretical predictions which have utilized Goulard's data for the surface reaction-rate parameters and the zero-pressure-gradient heat-transfer analysis. The effect of the Mach-number gradient on the measurements has been shown earlier to be small, a conclusion supported by Cohen & Reshotko, whose calculations give an increase in the shear stress of 5 % above the zero-pressure-gradient case for similar enthalpy ratios. A more significant observation made by the above authors is that heating the surface increases the sensitivity of the shear at the wall to external pressure gradients. This behaviour is extremely sensitive to the surface temperature and is probably contributing to the disagreement near the leading edge on all the heat-transfer curves. In addition, Janowitz & Libby (1965) indicate that significant alterations in the heat-transfer predictions result from accurate descriptions of the gas transport properties. Their results yield considerable errors in the theoretical heat-transfer predictions (up to 50 %) due to the use of various approximations for the transport properties; and show that these errors tend to increase with both surface temperature and free-stream dissociation fraction. This dependence of the theoretical predictions on the approximations being used for the transport properties may well be a significant factor in correlating the results with the heat-transfer observations.

When the results from the heat-transfer data to the catalytic and non-catalytic surfaces are compared, a substantial reduction is seen to occur for the low cata-

lyticity surface. For the high enthalpy levels the heat-transfer rate is some 50 % less than in the catalytic wall case. For free-stream dissociation fractions below 0·10, the copper surface absorbs 35 % more heat than the non-catalytic wall. This discrepancy is caused principally by the insulating effect of the oxide layer, which is 20 % of the total material thickness, and has a thermal conductivity that is (1/130) that of copper. The insulating properties of this layer cannot therefore be neglected, and a simple calculation indicates that for the test conditions the aluminium oxide reduces the measured heat-transfer rates by some 30 %, throughout the enthalpy range.

6. Conclusions

(1) The non-equilibrium laminar boundary-layer flow produced by a supersonic arc-heated wind tunnel has been studied in some detail for nitrogen and argon gases. The small scale of the facility has restricted the test region to less than an inch in the axial direction. However, within this régime the flow field has been shown to be two-dimensional. The observed boundary-layer thicknesses compare favourably with the theoretical calculations based on the assumption of chemically frozen isentropic nozzle flow.

(2) The similarity of the boundary-layer profiles has been established in partially dissociated flow fields. When the profile measurements are compared with the Chapman–Rubensin theory substantial differences occur, which are attributable to both the effects of a finite pressure gradient and significant dissociation fractions. It is estimated that between 6 and 10 % of the discrepancy is due to the dissociative effects which have a direct influence on the transport properties of the gas.

(3) Varying the probe dimensions to account for the vorticity in the shear layer has been shown to have only a small effect on the measured pressure distributions in the boundary layer; at most 6 % for the cases considered.

(4) When the diffusive heat-transfer contribution is taken into account the experimental measurements in the dissociated nitrogen flow are comparable to the theoretically estimated results. The reaction-rate constant apparently increases significantly above the values predicted by Goulard (1958), when the surface temperature is raised.

(5) The application of a non-catalytic aluminium oxide layer has been shown to reduce the heat-transfer rates substantially. Allowing for the oxide layer's insulating effects, there is approximately 15 % less heat transfer to the non-catalytic surface at the high enthalpies. Values for the surface reaction-rate parameter some ten times larger than Goulard's have been utilized to increase the theoretical predictions. If these values are realistic for the experimental work, a possible explanation is that the porous oxide surface became impregnated with a copper deposit originating from the electrode contamination that exists in the free-stream.

(6) Finally it must be emphasized that the accuracy of all of the theoretical analysis is dependent on approximations being used to describe the behaviour of the transport properties. The observations agree with the trends indicated by

Janowitz & Libby for the dependence of the boundary-layer profiles and the surface heat-transfer rate on the free-stream dissociation fraction.

The author is indebted to Mr J. L. Stollery and Dr J. K. Harvey for their encouragement and many stimulating discussions on the topics described herein. The valuable criticisms of Dr K. N. C. Bray of Southampton University are also gratefully acknowledged.

This work formed part of a thesis submitted to the Engineering Faculty of the University of London in partial fulfilment of the requirements for the degree of Doctor of Philosophy.

REFERENCES

ADCOCK, B. D. & PLUMTREE, W. E. G. 1964 *J. Quant. Spect. Rad. Transfer*, **4**, 29–39.

AMDUR, I. & MASON, E. A. 1958 *Phys. Fluids*, **1**, 370–383.

ARAVE, R. J. 1963 *Boeing Aircraft Co. Rep.* no. D2-22291.

BOSNJAKOVIC, F., SPRINGE, W., KNOCKE, K. F. & BURGHOLTE, L. P. 1959 *Thermodynamic and Transport Properties of Gases, Liquids and Solids.* New York: ASME.

CHAMBRÉ, P. L. & ACRIVOS, A. 1956 *J. Appl. Phys.* **27**, 1322–1328.

CHAPMAN, D. R. & RUBESIN, M. 1949 *J. Aero. Sci.* **16**, 547–565.

CHENG, H. K., HALL, J. G., GOLIAN, T. C. & HERTZBERG, A. 1961 *J. Aero. Sci.* **23**, 353–382.

CHUNG, P. M., LIU, S. W. & MIRELS, H. 1963 *Int. J. Heat & Mass Transfer* **6**, 193–210.

COHEN, C. B. & RESHOTKO, E. 1956 *NACA Rep.* no. 1293.

DORRANCE, W. H. 1962 *Viscous Hypersonic Flows.* New York: McGraw-Hill.

FAY, J. A. & RIDDELL, F. R. 1958 *J. Aero. Sci.* **25**, 73.

FREEMAN, N. C. & SIMPKINS, P. G. 1965 *Quart. J. Math. & Appl. Mech.* **18**, 213–229.

GOULARD, R. 1958 *Jet Propulsion*, **28**, 737.

HARVEY, J. K. & SIMPKINS, P. G. 1962 *J. Roy. Aero. Soc.* **66**, 637–641.

HAYES, W. D. & PROBSTEIN, R. F. 1959 *Hypersonic Flow Theory.* New York: Academic Press.

HUMPHREY, R. L., LITTLE, W. J. & SEELEY, L. A. 1960 Mollier diagram for nitrogen. *Arnold Engineering Dev. Center* AEDC-TN-60-83.

JANOWITZ, G. S. & LIBBY, P. A. 1965 *Int. J. Heat & Mass Transfer*, **8**, 7–18.

LIGHTHILL, M. J. 1957 *J. Fluid Mech.* **2**, 1–32.

MONAGHAN, R. J. 1957 *Aero. Res. Counc. R & M* no. 3056.

PROK, G. M. 1963 *NASA TN.* no. D 1567.

SIMPKINS, P. G. 1965 Ph.D. Thesis, Imperial College, University of London.

VAN DRIEST, E. R. 1952 *NACA TN.* no. 2597.

VAS, I. & BOGDONOFF, S. M. 1959 *Princeton University Department of Aero. Rep.* no. 450.

WOOLLEY, H. W. 1956 *NACA TN.* no. 3271.

YOS, J. M. 1963 *AVCO RAD TM.* no. TM 63-7.